2014 IEEE/ASME International Conference on
Advanced Intelligent Mechatronics (AIM)
Besançon, France, July 8-11, 2014

Repulsive Reaction Vector Generator for Whole-Arm Collision Avoidance of 7-DoF Redundant Robot Manipulator

Ren C. Luo[1], Meng-Chu Ko[2], Yi-Ting Chung[3], Raja Chatila[4]

Abstract— **In this paper, we propose a repulsive reaction vector generator (RVG) for whole-arm collision avoidance of 7-DoF redundant robot manipulator, and elucidate the case of spherical-revolute-spherical (S-R-S) type manipulator. Furthermore, this article discusses the obstacle-avoiding function of RVG, in which the generated reaction vector can aid the manipulator to achieve collision avoidance in an intuitive way by taking arm angle as the redundant parameter. First of all, we use six representative points to describe the manipulator, and generate the repulsive vectors according to the relationship between obstacle and the tip, wrist, and arm body of the manipulator, respectively. Next, after the pose of the manipulator, including position, orientation, and arm angle, is rectified by the reaction vector, the command would be sent to proposed vOTG to complete the reactive motion. As a result, the manipulator can achieve intuitive repulsive reaction, active whole-arm collision avoidance, and meanwhile avoiding the minor-risk obstacle by rotating the arm plane. Experimental results with NTU-iCeiRA arm developed in our lab and Microsoft Kinect depth sensor are presented.**

I. INTRODUCTION

A. Motivation and Related Works

Collaboration and interaction between human and robot are thought to be one of the most important features of robotic applications, especially in the industrial technology, domiciliary service, and medical field. In the scenario of human-robot collaboration (HRC), robot would most likely share the same workspace with human beings when dealing with service and industrial tasks, such as tasks in assembly line, laboratory, or house. However, it cannot be denied that the closer robot and human are, the more safety issues would rise. In this reason, some researchers tried to design safety-oriented robot with compliant control [1], lightweight feature [2], artificial skin [3], or variable stiffness actuator (VSA) structure [4] to limit the potential injuries while unexpected collision occurs. Furthermore, due to the high cost of those extra apparatuses, lots of research tried to come up with how to avoid the obstacle collision beforehand, which is also called contactless avoidance reaction, and it is also the safest way to tackle the safety issues.

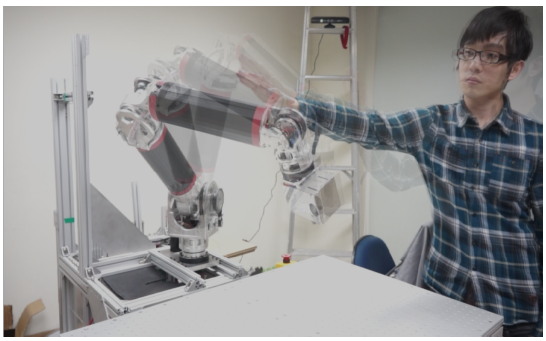

Fig. 1. Demonstration of active whole-arm collision avoidance with our designed 7-DoF harmonic driven 5kg payload robot manipulator in NTU-iCeiRA Lab.

Generally speaking, contactless avoidance reaction can be divided into two ways: (1) path planning algorithm and trajectory generation [5][6], and (2) reaction planning and motion generation [7][8][9]. The former approach plans a collision-free path, and then calculates the corresponding trajectory with spline, such as cubic, quadratic, or non-uniform rational B-Splines (NURBS). Also, this method mostly focuses on how to obtain more precise, time-optimal, and jerk-limited avoidance path. However, it is susceptible to the dynamical obstacle, and the computation often cannot be real-time. By contrast, the latter approach produces a reaction, which is usually from potential method, and then it computes the corresponding motion to achieve obstacle avoidance.

There are many researchers interested in the second method mentioned above. Among them, Torsten Kroger et al. achieved dynamic obstacle avoidance by applying Pivot Algorithm [9], which used the information of distance and velocity to construct an orthonormal base to calculate a better avoidance way. Furthermore, they use variable joint velocity constraints to passively avoid the body of manipulator while obstacle occurs nearby the arm body [10]. However, in the field of human-robot collaboration, an active arm body avoidance is requisite for a safety-oriented manipulator. Besides, an intuitive avoid pattern is also needed for collaborative service and industrial robot. As a result, in this paper, we present a repulsive reaction vector generator for 7-DoF redundant manipulator to achieve active whole-arm collision avoidance by taking arm angle as the redundant parameter. Furthermore, the vOTG is proposed to guarantee the continuous motion after the reaction vectors are generated. In this way, the

[1]Ren C. Luo is with the Center for Intelligent Robotics and Automation Research, National Taiwan University, No. 1, Sec. 4, Roosevelt Road, Taipei, Taiwan 106. (corresponding author to provide phone: +886-2-3366-9822; e-mail: renluo@ntu.edu.tw.)

[2]Meng-Chu Ko is with the Center for Intelligent Robotics and Automation Research, National Taiwan University, No. 1, Sec. 4, Roosevelt Road, Taipei, Taiwan 106. (e-mail: mhsiao@ira.ee.ntu.edu.tw.)

[3]Yi-Ting Chung is with the Center for Intelligent Robotics and Automation Research, National Taiwan University, No. 1, Sec. 4, Roosevelt Road, Taipei, Taiwan 106. (e-mail: yichung@ira.ee.ntu.edu.tw.)

[4]Raja Chatila is with UPMC/ISIR; 4 place Jussieu, CC 173, 75252 Paris cedex 05, France. (e-mail: chatila@isir.upmc.fr)

manipulator can achieve obstacle avoidance by rotating its arm plane, which is presented in section II-B, and also the avoiding pattern is more intuitive for human because the pose of the manipulator consists of the position, orientation, and arm angle of the manipulator exactly.

B. Paper Structure

This paper is organized as follows. To begin with, Section II illustrates the concept of the S-R-S model, arm plane, and analytical inverse kinematics solution of 7-DoF redundant manipulator, respectively. Section III elucidates the concept of RVG, and the algorithm of generating repulsive vector of the tip, wrist, and body of the manipulator, respectively. Section IV states the proposed vOTG and motion control. In Section V, experimental results with NTU-iCeiRA arm, as shown in Fig. 1, and Microsoft Kinect depth sensor are presented. Finally, we conclude in the Section VI.

II. PRELIMINARY KNOWLEDGE

In this section, concept of S-R-S model, arm plane, and analytical inverse kinematic solution are introduced. Furthermore, we describe the benefits of taking those attributes mentioned above into account in the following passage.

A. S-R-S model for 7-DoF Redundant Manipulator

Model is needed when analyzing the manipulator. However, since the kinematic equation is highly dependent on the manipulator structure, we firstly consider typical 7-DoF redundant manipulator by applying spherical-revolute-spherical (S-R-S) model. As shown in Fig. 2, there are three, one, and three revolute joints arranged from shoulder, elbow, and wrist, respectively. Due to the fact that three axes of shoulder joints intersect at a single point, the shoulder joints can be regarded as a virtual spherical joint. The wrist joints can also be treated as a spherical joint by the same reason. What's more, S-R-S manipulator is also known as an anthropomorphic arm because its similarity with a human arm. For the field of service and collaborative manipulator, it's suitable to apply this model and meanwhile without losing the generality.

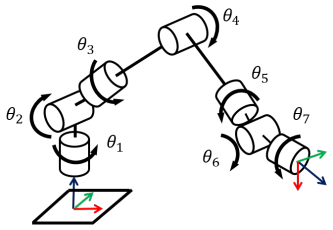

Fig. 2. S-R-S model for 7-DoF redundant manipulator

By applying S-R-S model mentioned above, we can simplify the representation of the 7-DoF redundant manipulator by six representative points as shown in the Fig. 3-(d). To further explain, the point S, P, E, A, W, and T stand for the shoulder, posterior limb, elbow, anterior limb, wrist, and tip of the manipulator, respectively. The point P is the mid-point between shoulder and elbow, and the point A is the mid-point between elbow and wrist.

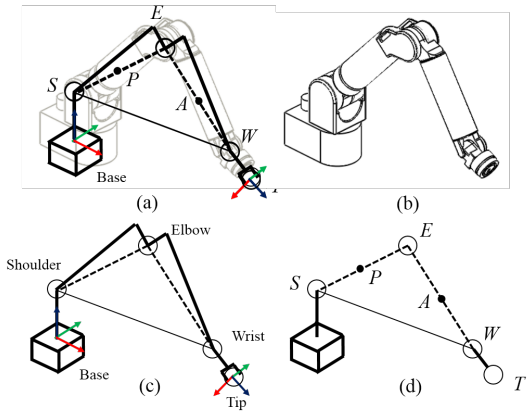

Fig. 3. (a) Hybrid illustration of the following pictures. (b) Original CAD picture, (c) Simplified linkage representation, and (d) Six representative points of 7-DoF redundant manipulator.

B. Arm Plane and Arm Angle

The arm plane, another important term in this paper, is a plane spanned by the point of the shoulder, elbow, and wrist of the manipulator, as shown in Fig. 4-(a), and the arm angle is defined as the angle between arm plane and reference plane, which is also a plane spanned by the point of shoulder, elbow, and wrist of the manipulator while the third joint equals to zero. Furthermore, since the arm angle is equivalent to the redundancy, the arm angle can be arbitrary chosen. This attribute makes the reaction of 7-DoF redundant manipulator be more intuitive since the whole freedom space consists of position of the tip (three), orientation of the tip (three), and arm angle (one) of the manipulator. Most importantly, taking arm angle into account allows the manipulator to avoid the minor-risk obstacle by rotating the arm plane. That is to say, when there exists a way for the manipulator to avoid obstacle with its arm angle, it can achieve obstacle avoidance by rotating the arm plane and meanwhile keep the position and orientation of the tip unchanged as shown in Fig. 4-(b) and (c).

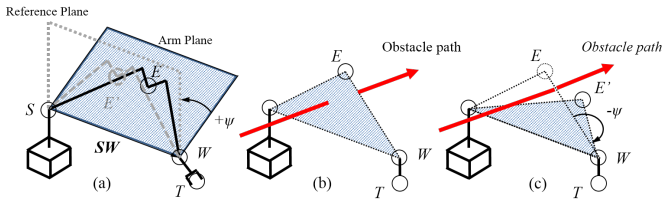

Fig. 4. (a) The illustration of the arm plane, where ψ stands for the rotation angle along SW axis, and counter clockwise direction donates the positive value. (b) Red line indicates the moving path of obstacle, and it has the risk of collision. (c) Robot arm can achieve object avoidance by rotating its arm plane, and meanwhile keep the position and orientation of tip unchanged.

C. Analytical Inverse Kinematic Solution

The analytical inverse kinematic solution of S-R-S type 7-DoF manipulator is based on [11] while the elbow offset is concerned. In this method, we can calculate the joint space

solution ($\theta 1 \sim \theta 7$) by choosing arbitrary position of the tip, orientation of the tip, and arm angle. To further explain, the angle of third joint 3 is firstly set to zero, and we can use geometric approach to compute the joint space solution. More details are provided in [**?**].

III. REACTION VECTOR GENERATOR

In this section, we elaborate the idea of overall system structure, information flow between each system block, and the algorithm of generating reaction vector, respectively. Furthermore, the vOTG and motion control are elucidated in next section. Noted that we only illustrate a simple case of repulsive reaction vector generator in this paper, and more discussions are in section VI.

A. Overall System Structure

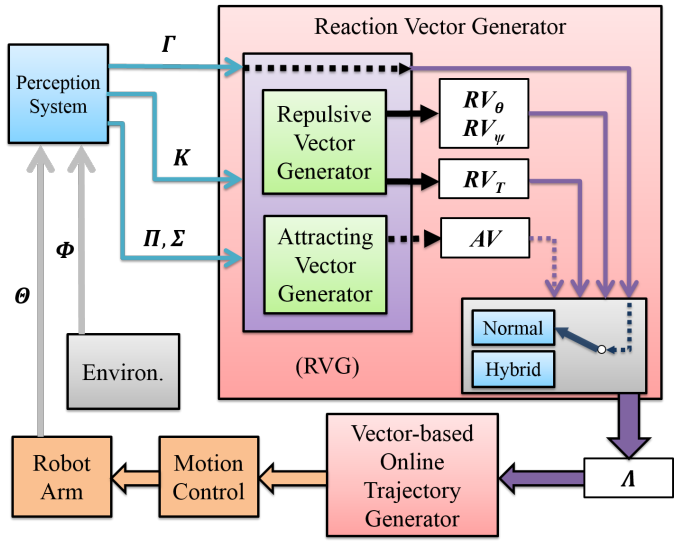

Fig. 5. Overall system structure with RVG and vOTG

Figure 5 shows the overall system structure including RVG, and we describe the information flows between each block as follows. To begin with, the perception system can transmit information between the manipulator and dynamic environment to the RVG while the information may be from the exteroceptive sensor (e.g. camera, laser-range finder, or depth-information sensor) or the proprioceptive sensor (e.g. encoder, force/ torque sensor, or Inertial measurement unit (IMU)). We mark the information acquired from exteroceptive sensor as $\mathbf{\Phi}$, and those from proprioceptive sensor as $\mathbf{\Theta}$, respectively. Furthermore, for the input of RVG, the $\mathbf{\Gamma}$ presents the mode selection, i.e. $\mathbf{\Gamma}$ = {selection of modes}, and the $\boldsymbol{K}$ indicates the weighting of different obstacles, i.e. $\boldsymbol{K}$ = $\{K_{ob1}, K_{ob2} \ldots K_{obn}\}$, where n means the weighting of number n obstacle. Also, the $\mathbf{\Pi}$ and $\mathbf{\Sigma}$ stand for the collective information of relationship between obstacle and the tip as well as the arm body, respectively, i.e. $\mathbf{\Pi}$ = {info. between obstacle and arm body} and $\mathbf{\Sigma}$ = {info. between obstacle and the tip}, where the information could be the distance or relative velocity between obstacle and representative points of arm. On the other hand, for the output of RVG, the $\mathbf{\Lambda}$ indicates the collection of resulting reaction vectors, and these vectors can be treated as the reference command of position, velocity, or acceleration for vOTG as a target to generate continuous motion command. Finally, after generating the smooth trajectory by vOTG, we apply motion control to follow the reference trajectory and achieve active whole-arm collision avoidance.

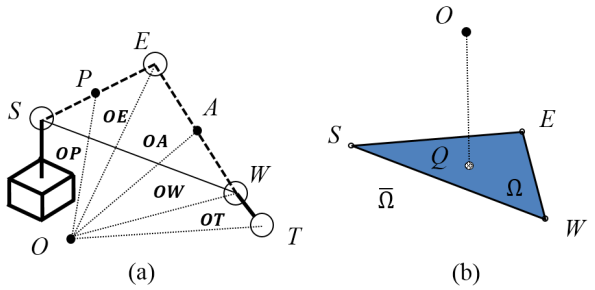

Fig. 6. (a) Representative points on the arm plane and their relationship between obstacle and themselves. (b) Q is the projecting point of obstacle point O on the triangular area $\mathbf{\Omega}$, which is on the arm plane.

B. Problem statement

In this paper, we firstly discuss a simple case by: (1) only considering the distance information and (2) using six points to represent manipulator as shown in Fig. 6-(a). Furthermore, **OP**, **OE**, **OA**, **OW** and **OT** indicate the vector from obstacle to the representative point of arm, i.e. $\mathbf{\Pi}$ ={**OP**,**OE**,**OA**,**OW**} and $\mathbf{\Sigma}$ ={**OT**}. Finally, we assume the weightings of different obstacles are equal, i.e. $\mathbf{\Omega}$ ={1,1 …}, and this would be discussed in section VI. On the other hand, as shown in Fig. 6-(b), the triangular area $\mathbf{\Omega}$ is comprised of S, E, and W, and it is on the arm plane. The complementary space of $\mathbf{\Omega}$ on the arm plane is $\bar{\Omega}$, and Q is the projecting point of obstacle point O on the $\mathbf{\Omega}$.

C. Repulsive vector

In this subsection, three types of repulsive vector are presented. To begin with, repulsive vector of the tip, $\mathbf{RV_T}$, is designed to reduce the risk of collision of the end-effector by influencing the position of the tip, x, y, and z (DoF 1, 2, and 3). On the other hand, the repulsive vector of the wrist, $\mathbf{RV}_\theta$, and the repulsive vector of arm body, $\mathbf{RV}_\psi$, are devised to achieve active collision avoidance of arm body by rectifying the orientation, α, β, and γ (DoF 4, 5, and 6), of the tip and arm angle, ψ (DoF 7).

1) Repulsive vector of the tip ($\mathbf{RV_T}$): For the collision avoidance, the most important task is to keep the tip from unexpected impact. Therefore, for the repulsive vector of the tip, marked as $\mathbf{RV_T}$, we use a simple but effective method to generate it with a logistic function. To explain, we consider the information data in $\Sigma = \{\mathbf{OT}\}$ and it is defined as

$$\mathbf{RV_T} = rv(\|\mathbf{OT}\|)\frac{\mathbf{OT}}{\|\mathbf{OT}\|} \tag{1}$$

$$rv(d) = D_{max}[\frac{1}{2} + \frac{1}{2}\tanh(4\rho - 8d)], \quad (2)$$

where the magnitude of the repulsive vector is given by a logistic function, in which D_{max} is the maximum admissible moving distance value, and ρ is the shaping factor. As shown in Fig. 7, the repulsive magnitude will be D_{max} when d equals to zero, and will approach to zero if the distance decreases to ρ[m].

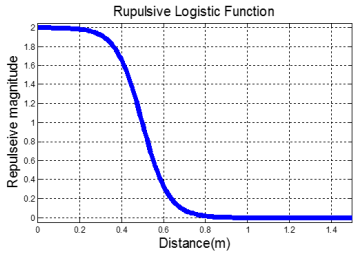

Fig. 7. Repulsive magnitude from (2), with parameters D_{max}=2[m] and ρ=1[m].

2) Repulsive vector of the wrist ($\mathbf{RV}_\theta$): The repulsive vector of the wrist can be computed by the following procedure. First of all, we choose the minimum of $\mathbf{\Pi}$ ={**OP**,**OE**,**OA**,**OW**} and mark it as **OX**, where X is the nearest representative point to the obstacle. Later, we can calculate the repulsive vector of X, $\mathbf{RV_X}$, by (1) and (2). Next, the direction and the magnitude of $\mathbf{RV}_\theta$ can be given by

$$Direction(\mathbf{RV}_\theta) = \mathbf{u_{wt}} \times \boldsymbol{\mu} \quad (3)$$

$$Magnitude(\mathbf{RV}_\theta) = \mathbf{k}_\theta \|\mathbf{WT} \times \boldsymbol{\mu}\| = \boldsymbol{\omega}, \quad (4)$$

where $\boldsymbol{\mu}$ equals to the subtraction of $\mathbf{RV_T}$ from $\mathbf{RV_X}$; **WT** and $\mathbf{u_{wt}}$ are the vector and unit vector from the wrist to tip, respectively; $\mathbf{k}_\theta$ is a shaping value. Finally, we can rectify the orientation of the tip by multiplying a rotation matrix as follows.

$$R_\theta = I_{3\times3} + \sin\omega[\,S(u_{wt\times\mu})\,] + (1-\cos\omega)[\,S(u_{wt\times\mu})\,]^2 \quad (5)$$

$$R_{i+1} = R_\theta R_i, \quad (6)$$

where S() is the skew symmetric matrix, and R_i *and* R_{i+1} are the original and rectified orientation, respectively.

3) Repulsive vector of arm body ($\mathbf{RV}_\psi$): As section II states, the arm angle can be treated as redundant parameter of the manipulator, and therefore the active whole-arm collision avoidance can be achieve by rotating the arm plane with the $\mathbf{Ap}_\psi$. The repulsive vector of arm body can be computed by the following procedure. First of all, we compute the projecting point Q on the $\mathbf{\Omega}$ as shown in Fig. 6-(b). Later, the direction and the magnitude of $\mathbf{RV}_\psi$ can be given by

$$\mathbf{RV}_\psi = rv\,(\sqrt{\|\mathbf{OX}\|^2 + \|\mathbf{OQ}\|^2})\,\mathbf{u}_\psi \quad (7)$$

$$\mathbf{u}_\psi = \begin{cases} +\mathbf{u_{SW}} & ,\textit{if}\ (\mathbf{u_{SE}} \times \mathbf{u_{EW}}) \cdot \mathbf{u_{OQ}} = +1 \\ -\mathbf{u_{SW}} & ,\textit{if}\ (\mathbf{u_{SE}} \times \mathbf{u_{EW}}) \cdot \mathbf{u_{OQ}} = -1, \end{cases} \quad (8)$$

where $\mathbf{u_{SE}}, \mathbf{u_{EW}}, \mathbf{u_{SW}}$,and $\mathbf{u_{OQ}}$ are the unit vector of the shoulder to the elbow, the elbow to the wrist, the shoulder to the wrist, and the obstacle point to the corresponding projecting point, respectively.

D. Reaction Vector

Finally, the resulting reaction vector $\mathbf{\Lambda}$, which contains $\mathbf{RV_T}, \mathbf{RV}_\theta, \textit{and}\ \mathbf{RV}_\psi$ in this case, is generated as the output of reaction vector generator. This can be treated as a reference command to achieve obstacle avoidance. However, these command will be discrete and jerky, and sometimes they might lead an unstable movement for extreme situations. To solve this problem, we use vector-based online trajectory generator to smooth the trajectory command, and this will be elucidated in next section.

IV. TRAJECTORY GENERATION AND MOTION CONTROL

In this section, we discuss how reaction vector obtained from previous section can be used to modify robot motion and how to guarantee continuous motions with vOTG.

A. Active Whole-Arm Collision Avoidance

First, we consider to command the robot arm at the joint position level. The given task for the manipulator is to actively avoid the obstacles while an obstacle is detected nearby the manipulator. The reaction vector is generated by means discussed in previous section, and the new command will be

$$\mathbf{x_{i+1}} = \begin{bmatrix} \mathbf{x} \\ \mathbf{y} \\ \mathbf{z} \\ \alpha \\ \beta \\ \gamma \\ \psi \end{bmatrix}_{i+1} = \mathbf{x_i} + \mathbf{RV}(\mathbf{P_{o,closest}}) = \mathbf{x_i} + \begin{bmatrix} \mathbf{RV_T} \\ \mathbf{RV}_\theta \\ \mathbf{RV}_\psi \end{bmatrix}, \quad (9)$$

where the $\mathbf{P_{o,closest}}$ is the closest obstacle point to the manipulator, and $\mathbf{RV}(\mathbf{P_o})$ is the reaction vector according to the obstacle $\mathbf{P_o}$. After the motion is rectified by the reaction vector, and new command will be sent to vector-based online trajectory generator, which is an intermediate layer between reaction vector generator and motion controller, as a new target command until the next new command is updated.

B. Vector-Based Online Trajectory Generator

Since the reaction vector is very reactive, the reactive avoidance must be jerky. Also, the motion, produced by directly sending command to the controller, might give the human the feeling of unsafe motion. Therefore, continuous motions with constrained velocity and acceleration are needed to achieve intuitive and safe repulsive reaction. In order to generate smooth trajectory, some researcher achieve online trajectory generator (OTG) by separating every degree of freedom and computing new command with time synchronized and phase synchronized method [12], whose motion can keep the proportional Cartesian displacement, i.e. draw a straight line.

In our work, we present vOTG, which consider vector as a basic element, and this can achieve proportional Cartesian movement in a simple way. As shown in the Algorithm 1, the input of this algorithm is the vector of target, current

command, variation of current command, and maximum permissive acceleration. On the other hand, the output is new command and variation of new command. To further explain, this algorithm can be divided into three parts: (1) decide the direction of new vector (code 1∼9 row), (2) decide the magnitude of new vector (code 10∼19 row), and (3) generate the new vector command (code 20∼26 row). Furthermore, all position, orientation, and the arm angle use the same approach to generate a vector-based smoothed trajectory. Finally, the smoothed trajectory of joint space can be obtained by the analytical inverse kinematics solution discussed in section II-C.

Algorithm 1: Vector-based Online Trajectory Generator

Input: P^{target}, P_i^{cmd}, V_i^{cmd}, a_{limit}
Output: P_{i+1}^{cmd}, V_{i+1}^{cmd}

1 **while** $MoveFlag = true$ **do**
2 $\quad \Delta P = P^{target} - P_i^{cmd}$;
3 $\quad$ **if** $(\|\Delta P\| \to 0)$ **then**
4 $\quad\quad$ **if** $(V_i^{cmd} \to 0)$ **then**
5 $\quad\quad\quad$ direction$(V^{target}) = \vec{0}$;
6 $\quad\quad$ **else**
7 $\quad\quad\quad$ direction$(V^{target}) = V_i^{cmd}/\|V_i^{cmd}\|$;
8 $\quad$ **else**
9 $\quad\quad$ direction$(V^{target}) = \Delta P/\|\Delta P\|$;
10 $\quad$ **if** $(\|\Delta P\| < \frac{1}{2}a_{limit}) \wedge \|V_i^{cmd}\| < a_{limit}$ **then**
11 $\quad\quad P_{i+1}^{cmd} = P^{target}$; $V_{i+1}^{cmd} = \vec{0}$;
12 $\quad\quad MoveFlag = false$;
13 $\quad$ **else**
14 $\quad\quad V_{max} = \sqrt{2\|\Delta P\| a_{limit}}$;
15 $\quad\quad \|V^{target}\| = \|\Delta P\|$; $a^{target} = \|\Delta P\| - \|V_i^{cmd}\|$;
16 $\quad\quad$ **if** $(\|\Delta P\| > V_{max}) \wedge (-a_{limit} < a^{target} < a_{limit})$ **then**
17 $\quad\quad\quad$ deceleration with a_{limit};
18 $\quad\quad$ **else if** $(\|\Delta P\| < V_{max}) \wedge (-a_{limit} < a^{target} < a_{limit})$ **then**
19 $\quad\quad\quad$ acceleration with a_{limit};
20 $\quad V^{target} = \|V^{target}\| \times$ direction(V^{target});
21 $\quad V_{i+1}^{cmd} = V^{target}$; $\Delta V = V^{target} - V_i^{cmd}$;
22 $\quad$ **if** $\|\Delta V\| \to 0$ **then**
23 $\quad\quad V_{i+1}^{cmd} = V_i^{cmd}$;
24 $\quad$ **else if** $\|\Delta V\| > a_{limit}$ **then**
25 $\quad\quad V_{i+1}^{cmd} = V_i^{cmd} + a_{limit} \times \frac{V_i^{cmd}}{\|V_i^{cmd}\|}$;
26 $\quad P_{i+1}^{cmd} = P_i^{cmd} + \frac{3}{2}V_{i+1}^{cmd} - \frac{1}{2}V_i^{cmd}$;

V. EXPERIMENTAL RESULTS

A. Experimental Setup

In the experiment of active whole-arm collision avoidance, the robot work space is monitored by a Microsoft Kinect depth sensor, positioned at a horizontal distance of 1.85 meters and at a height of 1 meter w.r.t. the robot base coordinate. The Kinect captures 640x480 depth image at a frequency of 30 Hz. After removing the manipulator from the image, the closest point nearby the manipulator is used to generate reaction vector. Later, new command is updated in every 120 ms, and sent to the vector-based online trajectory generator to produce joint position command in every 1ms, which guarantees the continuous motion which perform avoidance reaction. Furthermore, experiments are conducted on our own designed and developed 7-DoF robot manipulator 5kg payload in NTU-iCeiRA lab as shown in Fig. 1. Also, the implementation of the proposed reaction strategy is executed on a PC-based system with real-time kernel, and the control system includes gravity compensation and impedance control.

B. Experimental Results

First of all, for the following figures, the parameters used for the active whole-arm collision avoidance are $D_{max} = 0.8[m], \rho = 0.25[m], and\ k_\theta$ =1. Furthermore, the red, blue, and green hollow circles refer to the commands of the tip, wrist, and elbow of manipulator, respectively. The red, blue, and green lines stand for the trajectories of the tip, wrist, and elbow of manipulator, respectively. Also, the light blue hollow circle is the closest obstacle point in (9).

1) Experiment 1: Obstacle Avoidance of the Tip: In experiment 1, the scenario is that obstacles were detected nearby the tip of the manipulator, and the collision between human and manipulator would be avoided as shown in Fig. 8-(a) and Fig. 9-(a).

2) Experiment 2: Obstacle Avoidance of the Wrist: As shown in Fig. 8-(b) and Fig. 9-(b), experiment 2 considers the active whole-arm collision avoidance while the obstacle point is detected nearby the elbow of the manipulator. When the obstacle approaches to the wrist of manipulator, the avoidance reaction is firstly achieved mainly by rectifying the orientation of the tip, and then by the position of the tip. That is to say, the avoidance reaction turned from slight to significant one while the distance between obstacle and the tip is too small.

3) Experiment 3: Obstacle Avoidance of Arm Body: Figure 8-(c) and Fig. 9-(c) show similarly result with experiment 2 while the obstacle points occurred nearby the elbow of the manipulator. The obstacle avoidance is accomplished mainly by rotating the arm plane of the manipulator.

4) Experiment 4: Obstacle Avoidance of Minor-risk Obstacle: Finally, the experiment 4 illustrates the scenario mentioned in section II-B, which the obstacle avoidance can be achieved while the position and the orientation of the tip are unchanged with proper model selection as shown in Fig. 8-(d) and Fig. 9-(d).

VI. CONCLUSION

We present a reaction vector generator (RVG) for 7-DoF redundant manipulator, and discuss the obstacle avoiding scenarios for S-R-S manipulator. With proposed RVG and

Fig. 8. (a)-(d) show the image flows of the experiment 1 to 4. The robot perform avoidance while the obstacle is detected nearby (a) the tip of the manipulator, (b) the wrist of the manipulator, and (c) the arm body of the manipulator. Furthermore, (d) is the case of the obstacle is detected nearby the arm body of the manipulator, and meanwhile the position and orientation of the tip are unchanged.

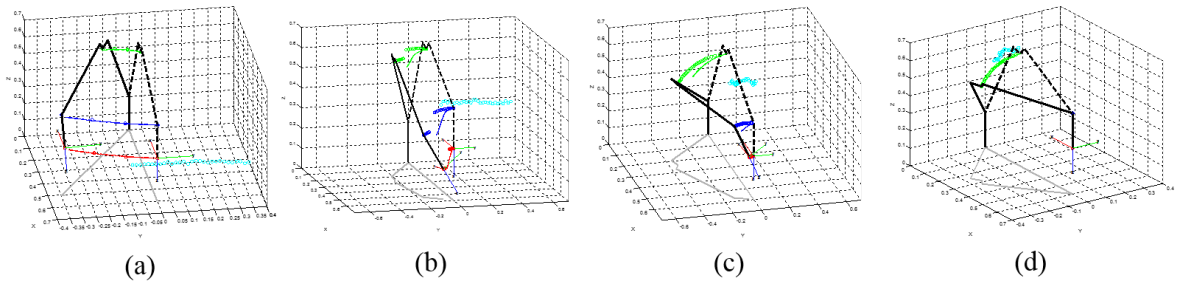

Fig. 9. (a)-(d) are the commands and trajectories of the tip, wrist, and elbow of the manipulator in the experiment 1 to 4, respectively. The red, blue, and green lines stand for the trajectories of the tip, wrist, and elbow of the manipulator, respectively. The light blue hollow circle is the closest obstacle point.

vOTG, active whole-arm collision avoidance is achieved by giving motor controller the smoothed reactive trajectory command while dynamic obstacle occurs. Also, in the scenario of avoiding minor-risk obstacle, the collision avoidance is achieved by rotating the arm plane of manipulator while the position and orientation of the tip kept unchanged. Moreover, further improvement in terms of intuitive robot behavior are obtained by taking arm angle as the redundant parameter of manipulator, and this should be the key feature of service collaborative robot in the future.

REFERENCES

[1] S. G. Khan, G. Herrmann, T. Pipe, C. Melhuish, and A. Spiers, "Safe adaptive compliance control of a humanoid robotic arm with anti-windup compensation and posture control," in *International Journal of Social Robotics*, vol. 2, pp. 305-319, 2010.

[2] A. Bicchi and G. Tonietti, "Fast and soft-arm tactics robot arm design," in *IEEE Robotics and Automation Magazine*, vol. 11, pp. 22-33, 2004.

[3] M. W. Strohmayr, H. Worn, and G. Hirzinger, "The DLR Artificial Skin Step: Uniting Sensitivity and Collision Tolerance," in *IEEE International Conference on Robotics and Automation*. (ICRA '13)

[4] A. De Luca, F. Flacco, A. Bicchi, and R. Schiavi, "Nonlinear decoupled motion-stiffness control and collision detection/reaction for the VSA-II variable stiffness device," in *IEEE/RSJ International Conference on Intelligent Robots and Systems*. (IROS '09), St. Louis, MO, USA, Oct. 11-15, 2009, pp. 5487-5494.

[5] J. van den Berg, D. Ferguson, and J. Kuffner, "Anytime path planning and replanning in dynamic environments," in *Proceedings IEEE International Conference on Robotics and Automation*, (ICRA '06), Orlando, Florida, USA, May 15-19, 2006, pp. 2366-2371.

[6] Y. Qian and A. Rahmani, "Path planning approach for redundant manipulator based on Jacobian pseudoinverse-RRT algorithm," in *International Conference on Intelligent Robotics and Applications, (ICIRA '13)*, Busan, Republic of Korea, Sep.25- 28, 2013, pp. 706-717.

[7] S. Haddadin, H. Urbanek, S. Parusel, D. Burschka, J. Rossmann, A. Albu-Schaffer, and G. Hirzinger, "Real-time reactive motion generation based on variable attractor dynamics and shaped velocities," in *IEEE/RSJ International Conference on Intelligent Robots and Systems (IROS '10)*, Taipei, Taiwan, Oct. 18-22, 2010, pp. 3109-3116.

[8] H. Reimann, I. Iossifidis, and G. Schoner, "Generating collision free reaching movements for redundant manipulators using dynamical systems," in *IEEE/RSJ International Conference on Intelligent Robots and Systems (IROS '10)*, Taipei, Taiwan, Oct. 18-22, 2010, pp. 5372-5379.

[9] F. Flacco, T. Kroger, A. De Luca, and O. Khatib, "A depth space approach to human-robot collision avoidance," in *IEEE International Conference on Robotics and Automation (ICRA '12)*, St. Paul, MN, USA, May 14-18, 2012, pp. 338-345.

[10] F. Flacco, A. De Luca, and O. Khatib, "Motion control of redundant robots under joint constraints: Saturation in the null space," in *IEEE International Conference on Robotics and Automation (ICRA '12)*, St. Paul, MN, USA, May 14-18, 2012, pp. 285-292.

[11] M. Shimizu, H. Kakuya, W.-K. Yoon, K. Kitagaki, and K. Kosuge, "Analytical inverse kinematic computation for 7-DOF redundant manipulators with joint limits and its application to redundancy resolution," in *IEEE Transactions on Robotics*, vol. 24, pp. 1131-1142, 2008.

[12] T. Kroger, "Online trajectory generation: Straight-line trajectories," in *IEEE Transactions on Robotics*, vol. 27, pp. 1010-1016, 2011.